J Solid State Electrochem (2006) 10:833–840
DOI 10.1007/s10008-006-0170-7

ORIGINAL PAPER

Nucleation-growth kinetics of the oxidation of silver nanocrystals to silver halide crystals

Ulrich Hasse · Stephen Fletcher · Fritz Scholz

Received: 24 April 2006 / Revised: 26 April 2006 / Accepted: 5 May 2006 / Published online: 8 June 2006

Abstract The electrochemical oxidation of silver nanocrystals to silver halide crystals proceeds by a process of nucleation and growth. The mechanism is confirmed by analyzing chronopotentiograms using a new extension of nucleation theory. The theory makes it possible to derive plots of nucleation-growth currents vs potential, and growth rates vs potential, directly from experimental data. Such plots yield powerful insights into the reaction kinetics. In situ AFM imaging reveals that a few thousand of silver nanocrystals are oxidized to only a few tens of silver halide crystals, *without pronounced loss of active material*. The mechanism of this remarkable process is described in this paper. In particular, it is shown that the decrease in crystal population proceeds via an oversaturated silver solution, i.e., a process that is mediated by "driven" Ostwald ripening across the electrode surface. At the same time, the low solubility of silver species in bulk solution means that few silver ions escape from the surface. This combination of features explains why the transformation from silver to silver halide is near-stoichiometric yet highly reconstructive.

Keywords Nucleation · Kinetics · Atomic force microscopy · Electrochemistry · Silver · Silver halides · Coup de fouet

Dedicated to our friend and colleague Professor Dr. Alan Bond on the occasion of his 60th birthday

U. Hasse · F. Scholz (✉)
Institut für Biochemie, Universität Greifswald,
Soldmannstrasse 23,
17489 Greifswald, Germany
e-mail: fscholz@uni-greifswald.de

S. Fletcher
Department of Chemistry, Loughborough University,
Ashby Road,
Loughborough, Leicestershire LE11 3TU, UK
e-mail: Stephen.Fletcher@lboro.ac.uk

Introduction

Electrochemically induced phase transformations of nanocrystals and microcrystals are of great interest industrially, mainly because of their technical importance in photography, energy storage, microelectronics, and in electrometallurgical processing (electrowinning and electrorefining). They are also of great interest from a fundamental point of view, because the theory of ion transfer is far less developed than the theory of electron transfer.

In general, phase transformations in nanocrystals differ *topologically* from phase transformations in bulk materials, because nanocrystals lack grain boundaries and have a small number of atoms. Additionally, phase transformations in nanocrystals also differ *kinetically* from phase transformations in bulk materials due to the accessibility of unusual kinetic regimes such as those associated with enhanced diffusional flux through non-planar diffusion zones, or higher-than-usual nucleation overpotentials due to the diminished number of active sites. Taken together, these topological and kinetic factors make nanocrystals a fascinating (and challenging) topic for research.

The present study is aimed, in part, at extending the theory of nucleation-growth kinetics [1] to electrochemically induced solid-state-phase transformations in nanocrystals. It is also intended as a contribution to the field of silver and silver halide colloids [2, 3]. Although the solid state oxidation of silver metal to silver halides has long been of interest to electrochemists [4–7], the in situ

imaging of individual silver nanocrystals has become possible only recently, due to the development of atomic force microscopy (AFM). For example, with the help of AFM, it has been discovered that the formation of silver halide crystals on "inert" gold electrodes is accompanied by a dramatic restructuring of the electrode surface [8]. In the present work, we initiate a kinetic analysis of these phenomena.

Experimental part

Instrumentation and electrodes

All measurements were performed with an AFM/STM manufactured by Digital Instruments (hardware: Nano-Scope Version 1.0; software: NanoScope E Version 4.23r3). A styropor box acoustically shielded the microscope, and a laboratory-built table was used to damp benchtop vibrations [9]. The electrochemical cell was externally controlled by a μ-AUTOLAB (EcoChemie, Netherlands). The electrochemical measurements were performed with the Autolab PGSTAT 20 (EcoChemie, Netherlands) and a VA-Stand 663 (Metrohm, Switzerland). Gold and platinum electrodes were used for AFM measurements, having been vapor-deposited on chromium-coated borosilicate glass (Schröer GmbH, Lienen, Germany). In the case of chronopotentiometric measurements, gold plates were used (electrode area 121 mm^2), and electrical contact was made via copper wires attached with silver epoxy glue (Type 3021B, Epoxy-Produkte, Fürth, Germany). The reference electrode was an Ag/AgCl (3 M KCl) electrode and all potentials in this paper refer to it (E=0.208 V vs SHE).

Chemicals

$AgNO_3$, ascorbic acid, KNO_3, KI, KBr, KCl, and H_2SO_4 (all p.a.) were from Merck (Darmstadt, Germany).

Synthesis of silver nanocrystals [8]

One hundred milliliters of a 5-M silver nitrate solution was mixed with 1 ml of a concentrated ammonia solution followed by a slow drop-wise addition of 200 ml of a 0.01-M freshly prepared ascorbic acid solution. During the addition of the ascorbic acid, the solution was slowly stirred. The resulting silver crystals were separated by centrifugation and resuspended in water. This process was repeated five times. After waiting for 120 s to allow any coarse particles to settle, one droplet of the final suspension was transferred to the electrode surface.

Immobilization of silver nanocrystals

One droplet of the silver nanocrystal suspension was transferred onto the surface of each gold and platinum electrode by means of a syringe. Typically, the electrodes had to be tilted in several directions to get an even coating. The coated surfaces were then evaporated to dryness in a drying oven at 45 °C. (Although we have recently shown that silver nanocrystals can also be deposited on gold electrodes via an Agar-Agar-templated reduction [10], we have not used that route in this study because we wanted to be sure that no traces of Agar-Agar were present on the surface of the silver crystals, because they could possibly affect the results.)

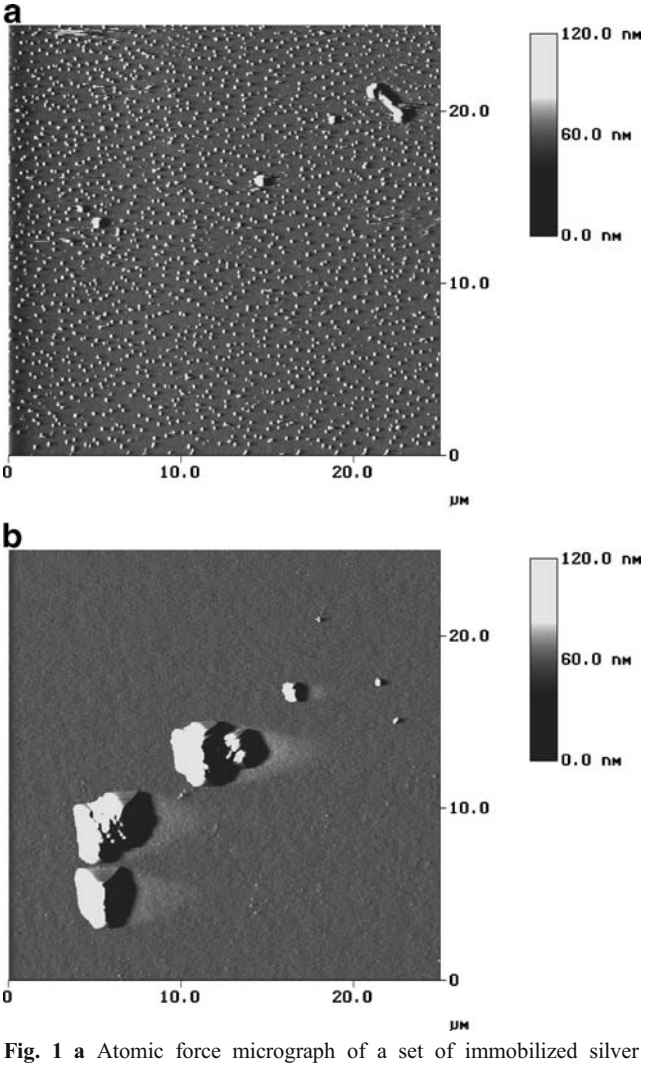

Fig. 1 **a** Atomic force micrograph of a set of immobilized silver nanocrystals before oxidation, and **b** after potentiostatic oxidation at E=0.1 V vs Ag/AgCl for 5 min. Electrolyte solution: 10^{-4} mol l^{-1} KBr and 0.1 mol l^{-1} KNO_3

Results and discussion

AFM studies of the electrochemical oxidation of silver nanocrystals immobilized on a gold electrode

Figure 1 shows AFM images of silver nanocrystals immobilized on a gold electrode, and what happened to them after they were potentiostatically oxidized to silver bromide. It can be seen that a large decrease in the number of crystals occurred: the initial 1,656 silver crystals were transformed into only six silver bromide crystals! However, summing the volumes of the crystals revealed the surprising fact that the reaction was practically stoichiometric, i.e., *nearly all the silver atoms were incorporated into the large silver bromide crystals*.

During the AFM measurements, it was soon realized that galvanostatic control had practical advantages over potentiostatic control for the purposes of imaging, because galvanostatic control permitted direct manipulation of the crystal growth rate. However, to obtain a large set of galvanostatic data suitable for theoretical analysis it was necessary to perform numerous electrochemical experiments, and the gold film electrodes used for AFM were expensive. To minimize costs, therefore, the AFM gold film electrodes were replaced by bulk gold electrodes for these particular measurements, as they could easily be repolished. Happily, the immobilization of the silver nanocrystals worked equally well in both cases.

Galvanostatic studies of the electrochemical oxidation of silver nanocrystals immobilized on a gold electrode

Figure 2 shows chronopotentiometric data recorded during the galvanostatic oxidation of silver nanocrystals on a gold electrode. Three different halides were selected for study: chloride, bromide, and iodide. In each case, the oxidation currents and halide ion concentrations were chosen so that the oxidation would take about 10 s. As the gold electrodes with immobilized silver nanocrystals were heterogeneous electrodes, they possessed "mixed" potentials that could not easily be compared with theoretical values. A comparison of the end potentials (i.e., when all the silver had converted to silver halide on the gold electrode surface) with the potential of a pure silver wire covered with the same silver halide, showed deviations of at least 20 mV. Accordingly, we measured all potentials vs a conventional reference electrode.

The curves in Fig. 2 reach overpotentials that correspond to higher silver ion activities than those at equilibrium. However, the higher activities relax to the equilibrium values after the nucleation and growth of silver halide crystals. They are, therefore, nucleation overpotentials. These *experimentally determined* nucleation overpotentials are readily measured, but may be slightly biased by the fact that the final potentials are "mixed" potentials. Neverthe-

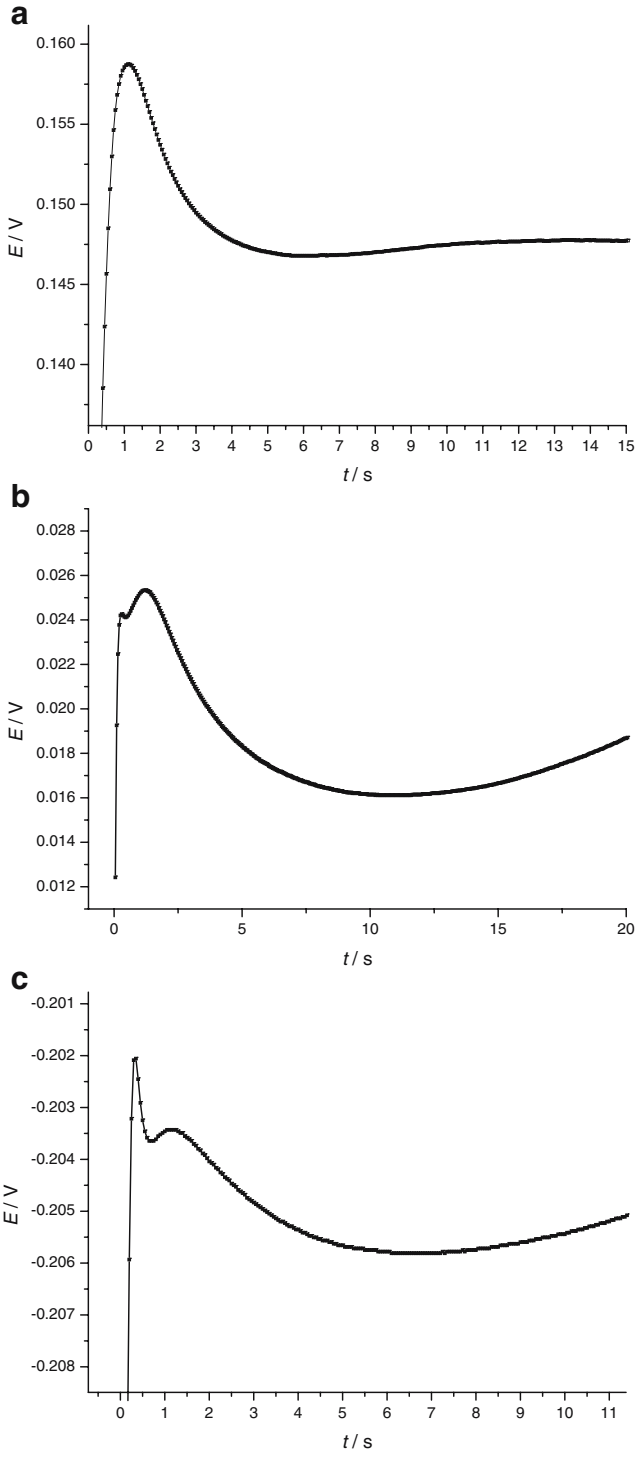

Fig. 2 Chronopotentiograms recorded during the oxidation of silver in solutions containing 0.1 mol l^{-1} KNO_3 and additionally 10^{-4} M KCl (**a**), KBr (**b**), and KI (**c**), respectively. The current was fixed at 2×10^{-4} A, and the geometrical surface area of the electrode was 121 mm^2

Table 1a Effect of halide identity on nucleation overpotentials (NOPs) in solutions containing 0.1 mol l^{-1} KNO_3

0.1 mol l^{-1} KNO_3+halide	Individual NOP [mV]	Average NOP [mV]
10^{-4} M KCl	13.1, 12.0, 16.6, 14.6	14.1
10^{-4} M KBr	8.1, 9.2, 7.8, 11.5	9.1
10^{-4} M KI	2.5, 4.3, 2.2, 3.8	3.2
10^{-4} M KCl saturated with AgCl	11.6, 13.4, 10.1	11.7
10^{-4} M KBr saturated with AgBr	7.0, 6.2, 7.4	6.9
10^{-4} M KI saturated with AgI	1.8, 1.5, 1.1	1.4
5×10^{-5} M KBr+5×10^{-5} M KI	6.12, 5.8, 5.8	5.9

less, we refer to them as the nucleation overpotentials, because the true values are inaccessible. (Obviously electrochemical measurements cannot be performed using silver macroelectrodes to immobilize the silver nanocrystals, because the silver macroelectrodes would be oxidized as well!) Independent of these caveats, each U-shaped potential-time curve always corresponds to a single nucleation-growth process.

In the case of silver bromide and silver iodide, *two* nucleation-growth processes were resolved, in accordance with the classical monolayer/bulk layer paradigm of anodic film formation reactions [11]. In the case of silver chloride, only one nucleation-growth process was resolved, which is probably an artefact of the time scale used. Tables 1a and 1b list the corresponding (maximum) nucleation overpotentials. The results shown in Tables 1a and 1b clearly demonstrate that the nucleation overpotential is higher when the equilibrium solubility is higher. This is also true for the mixed system containing silver chloride and silver bromide, which exhibited a nucleation overpotential intermediate between that of the pure chloride and pure bromide. Further, it is seen that pre-saturating the electrolyte solutions with the corresponding silver halides decreases the nucleation overpotentials.

Table 2 shows the nucleation overpotentials of oxidation of Ag to AgCl for different concentrations of chloride. The latter varied from 10^{-8} to 3 mol l^{-1}. At chloride concentrations smaller than 10^{-5} mol l^{-1}, no nucleation overpotentials could be determined as, obviously, no silver chloride could precipitate because the solubility product was not exceeded. Between 10^{-5} mol l^{-1} and 10^{-2} mol l^{-1} chloride the nucleation overpotentials grew, and at higher chloride concentrations they decreased. The latter effect must be due to the increased solubility of AgCl in chloride solutions caused by the formation of chloro complexes (log β_1=3.31, log β_2=5.25, log β_3=6.0) [12].

The chronopotentiometric data shown in Fig. 2 were the result of coupled double layer charging of the electrode and nucleation-growth of the new phase. The total current was, therefore,

$$I = C_{dl}\frac{dE}{dt} + \int_0^t I_1(\tau, t, E)N'(\tau, E)d\tau, \quad (1)$$

where C_{dl}=double layer capacitance, E=potential, t=time, I_1=current flowing into one crystal nucleated at time τ and observed at time t, and $N(\tau,E)$=potential-dependent appearance rate of crystals.

Equation 1 is an integro-differential equation of Volterra type, and so cannot be solved *analytically*. However, it is not difficult to separate the currents flowing into the two processes *empirically*, based on some reasonable assumptions. For example, at short times, it is reasonable to assume that all the applied current flows into double-layer charging and none into the nucleation-growth process, because the nuclei of the new phase are initially negligibly small. (This may also be justified by noting that the ascending branches of the chronopotentiograms are linear: in those regions only the first term in Eq. 1 is significant.) Thus, by measuring the slope of the initial part of a chronopotentiogram, an accurate estimate of C_{dl} may be obtained.

Armed with this estimate, it is then easy to solve for the partial current I_{dl} flowing into the double-layer-charging process throughout the entire chronopotentiogram. Furthermore, as it always holds that $I_{applied} = I_{dl} + I_{nucleation-growth}$, the corresponding partial current $I_{nucleation\text{-}growth}$ can be obtained by subtraction. Figure 3 shows some plots of $I_{nucleation\text{-}growth}$ for the oxidation of Ag crystals to AgCl, AgBr, and AgI. The presence of anti-clockwise "inductive" loops in these data immediately confirms our diagnosis of nucleation-growth kinetics [13]. Figure 4 depicts schematically how the nucleation-growth current vs potential curves are interpreted in case of AgBr and AgI; initially, there is a nucleation and growth of a monolayer of silver halide on

Table 1b Comparison of 1st and 2nd nucleation overpotentials

0.1 mol l^{-1} KNO_3+ added halide	1st NOP[mV]	2nd NOP[mV]	Average 1st NOP[mV]	Average 2nd NOP[mV]
10^{-4} M KBr	4.3, 0.15, 0.17, 2.3	7.6, 9.2, 8.9, 10.5	1.7	9.1
10^{-4} M KI	1.3, 2.9, 2.2, 1.6	3.6, 2.1, 1.7, 2.3	2.0	2.4

Table 2 Nucleation overpotentials for silver oxidation in solutions containing 0.1 mol l^{-1} KNO_3

Chloride concentration [mol/l]	NOP [mV]
10^{-8}	0
10^{-7}	0
10^{-6}	0
10^{-5}	5
10^{-4}	10.8
10^{-3}	12.5
10^{-2}	18.3
0.1	17.8
1	16.3
3	4

the silver crystals. The further rapid oxidation of the silver crystal destroys that monolayer and a thin solution layer is formed on the electrode surface, which is supersaturated with respect to the silver halide. From this supersaturated solution, via a second nucleation-growth process, silver halide crystals precipitate.

We may now summarize the shape of nucleation-growth chronopotentiograms as follows. The initial ascending branch is due to double-layer charging. The first descending branch is due to the increase of interfacial area associated with the combined effects of nucleation and growth. The broad minimum is due to near steady-state growth of the nucleated crystals, and finally the second ascending branch is due to the deceleration of the overall reaction, caused by depletion of reactant or diminution of active area.

It is pleasing to note that the above theory completes the matrix of possibilities by which nucleation/growth processes can be unambiguously identified. These are now summarized in the following table. (*Note*: By an "inductive loop," we mean any local region of the $I(E)$ plane where dE/dt is negative but dI/dt is positive.)

Stimulus	Response (diagnostic of nucleation/growth)
E=constant	Rising $I(t)$ transient
E (or I) cyclical	Inductive loop in $I(E)$ plot
I=constant	Falling $E(t)$ transient

It is particularly pleasing to observe that the above analysis also solves a problem of long standing in battery research, namely, the origin of the "*coup de fouet*" or "*whiplash*" effect [14]. This phenomenon, which has long been a puzzlement to researchers, appears as a sudden and dramatic voltage excursion during the early stages of charge or discharge of a battery (most famously the lead-acid battery). We note here that this is merely the expected behavior of Eq. 1, and corresponds physically to the system "searching" for a sufficiently high overpotential to nucleate and grow new crystals, if these have been severely depleted after a previous deep charge or discharge.

Returning now to Fig. 2, it is evident that the broad potential minimum in each chronopotentiogram corresponds to the situation when (1) the double-layer-charging process has finished, (2) the nucleation process has finished (here the second nucleation, i.e., nucleation of AgX crystals

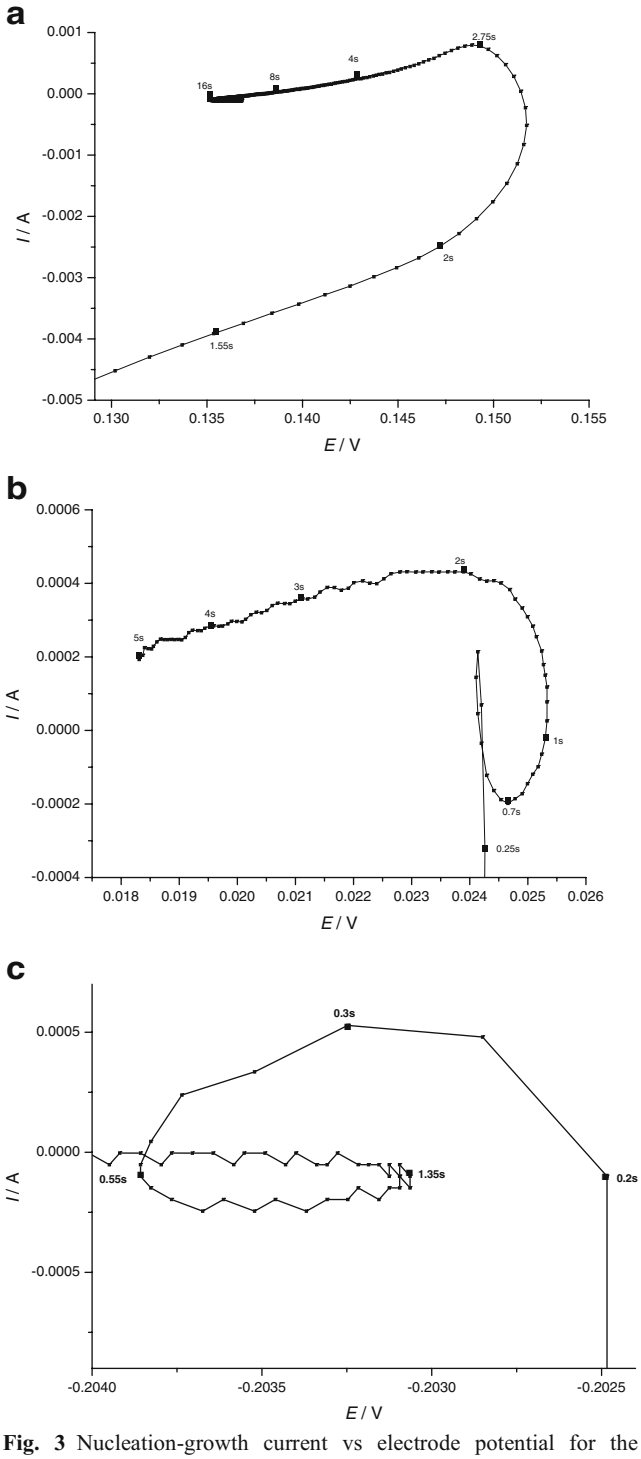

Fig. 3 Nucleation-growth current vs electrode potential for the measurement shown in Fig. 2a–c. **a** AgCl formation, **b** AgBr formation, and **c** AgI formation. The time elapsed since commencing the oxidation is indicated on the curves

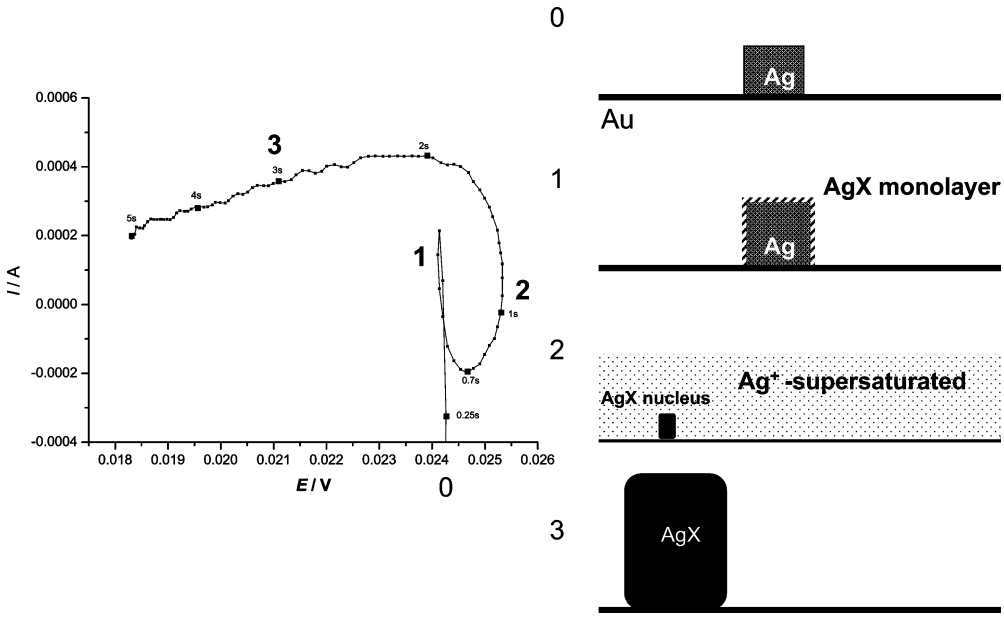

Fig. 4 Interpretation of the nucleation growth vs potential curve shown in Fig. 3b as a double nucleation process. This comprises the monolayer formation of silver halide on the silver crystal (at *1*), the bulk oxidation of the silver crystal to give a supersaturated silver halide solution (at *2*), and the final precipitation of the bulk silver halide on the electrode surface (at *3*)

from oversaturated solution), and (3) all the applied current is flowing into a fixed number of silver halide crystals, stimulating their growth. In this regime, it is possible to carry out a new kind of experiment, in which the applied currents are decreased stepwise, and the corresponding potentials are recorded (see Fig. 5a). By doing this, and then plotting each current vs potential, a current-voltage curve is obtained *for the growth process only* (see Fig. 5b).

Mathematically, this can be proved rather elegantly by operational calculus. Noting that the voltage excursion generates a brief but intense pulse of nucleation near $t \approx 0$, we make the approximation

$$N'(\tau) \approx N_0\ \delta\ (\tau), \tag{2}$$

where $N'(t)$ is the rate of nucleation (=dN/dt), N_0 is the total number of nuclei formed during the pulse, and $\delta(\tau)$ is Dirac's delta function. Substituting back into the full expression, i.e., Eq. 1,

$$I = C_{dl}\frac{dE}{dt} + \int_0^t I_1(\tau, t, E)N'(\tau, E)d\tau, \tag{3}$$

we immediately obtain

$$I = C_{dl}\frac{dE}{dt} + \int_0^t I_1(\tau, t, E)N_0\ \delta(\tau, E)d\tau. \tag{4}$$

However, at a broad potential minimum in the chronopotentiogram, $E \approx const.$ and so

$$I \approx N_0 \int_0^t I_1(t-\tau)\ \delta\ (\tau)d\tau. \tag{5}$$

Finally, by the *Umfaltung* property of convolution-type integrals, we obtain

$$I \approx N_0\ I_1 \tag{6}$$

Thus, at a broad potential minimum in a chronopotentiogram, the system attains a near steady-state growth regime in which the total current is approximately the current due to one crystal, multiplied by the total number of crystals N_0 formed during the pulse. It is interesting to note that this growth regime is inaccessible under simple potentiostatic conditions, although it can be attained in some cases by applying a large potentiostatic pre-pulse and then waiting long enough for non-steady state nucleation effects to decay away.

As

$$I_1 = nFA\ \left(k_f C_b - k_b\right) \tag{7}$$

where k_f is the rate constant of the forward (deposition) reaction, k_b is the rate constant of the backwards (dissolution) reaction, C_b is the bulk concentration of reactant, n is the number of electrons transferred per depositing ion, F is the Faraday constant, and A is the surface area of each individual crystal, we finally deduce that a plot of I vs E will, in effect, yield a plot of single crystal growth rate ($k_f C_b$–k_b) vs potential. In Fig. 5, it can be seen that the single crystal growth rate is a *linear* function of potential. Such a result is, in fact, diagnostic of reversible kinetics [13] for the interfacial ion transfer process at the nanocrystal surfaces.

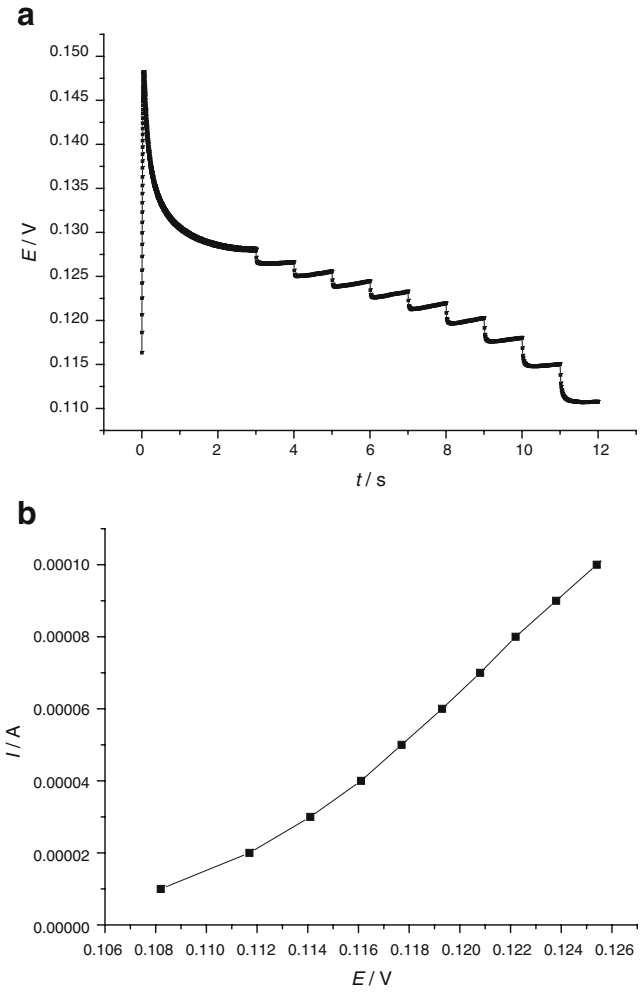

Fig. 5 **a** Chronopotentiometric trace of the oxidation of silver in a solution containing 0.1 mol l^{-1} KNO_3 and 10^{-4} M KBr solution under galvanostatic conditions. The current was fixed at 10^{-4} A for 3 s and afterwards reduced stepwise by 10^{-5} A each second. **b** shows the current vs potential plotted from the data in **a** using the final potential values of each step

Conclusions

In this study, we have shown that the oxidation of silver nanocrystals proceeds from a nucleation-growth mechanism. In some experiments, it was even possible to distinguish *two* nucleation processes—monolayer formation and bulk layer formation—as commonly observed in classical, macroscopic, and anodic film formation processes.

By extending electrochemical nucleation theory to galvanostatic conditions, we showed that it was possible to derive plots of nucleation-growth currents vs potential, and growth rates vs potential, directly from chronopotentiograms. Such plots, which are new, may be useful in future investigations of solid-state-phase transformations.

The drastic decrease in crystal population that accompanies the electrochemical oxidation of silver nanocrystals can be termed "driven" Ostwald ripening. This process is favored by a low supersaturation of dissolved species, which inhibits precipitation in solution. This lack of precipitation also explains why the phase transformation from silver to silver halide proceeds near-stoichiometrically.

Very recently we have shown that the chemical oxidation of silver nanocrystals by means of an aqueous solution of bromine yields results similar to electrochemical oxidation, provided that the silver nanocrystals are immobilized on a metal conductor (e.g., platinum) [15]: Out of a very large number of silver crystals, only a very small number of silver bromide crystals form. However, when the silver crystals are immobilized on an oxide non-conductor (quartz), nearly every silver crystal transforms into a silver bromide crystal. We suppose that, on platinum, a galvanic cell is created across the whole electrode surface, with bromine being reduced at the platinum and the silver nanocrystals dissolving rapidly to form a supersaturated solution. By contrast, on quartz, galvanic activity is restricted to the silver nanocrystal surfaces, so the reaction is much slower and more localized in that case.

Finally, we remark that the oxidation of immobilized silver nanocrystals to silver halides differs significantly from the reverse process, the reduction of immobilized silver halide crystals [16] (and indeed silver sulphide [17]) to metallic silver. In these cases, the nucleation of silver metal takes place at the three-phase junction where the silver halide crystal, the conducting substrate, and the solution meet.

Acknowledgements This project was supported by *Deutsche Forschungsgemeinschaft* and *Fonds der Chemischen Industrie*.

References

1. Milchev A (2002) Electrocrystallization; fundamentals of nucleation and growth. Kluwer, Boston
2. Kimijima K, Sugimoto T (2004) J Phys Chem B 108:3735
3. Jin R, Cao YW, Mirkin CA, Kelly KL, Schatz GC, Zheng JG (2001) Science 291:1901
4. Jin X, Lu J, Liu P, Tong H (2003) J Electroanal Chem 542:85, and references therein
5. Scholz F, Schröder U, Gulaboski R (2005) The electrochemistry of immobilized particles and droplets. Springer, Berlin Heidelberg New York
6. Vetter K (1961) Elektrochemische Kinetik. Springer, Berlin Heidelberg New York, p 571
7. Dignam MJ (1981) In: Bockris JO'M, Conway BE, Yeager E, White RE (eds) The kinetics of the growth of oxides, in comprehensive treatise of electrochemistry, electrochemical materials science, vol 4. Plenum, New York, p 291

8. Hasse U, Scholz F (2004) Electrochem Commun 6:409
9. Hasse U, Scholz F (2001) Electrochem Commun 3:429
10. Hasse U, Scholz F (2006) J Solid State Electrochem 10:380
11. Fletcher S (1981) J Electroanal Chem 118:419
12. Kotrlý S, Šùcha L (1985) Handbook of chemical equilibria in analytical chemistry. Ellis Horwood, Chichester, p 137
13. Fletcher S (1983) J Electroanal Chem 159:267
14. Pascoe PE, Anbuky AH (2002) J Power Sources 111:304
15. Hasse U, Scholz F (2006) Electrochem Commun (in press) DOI: 10.1016/j.elecom.2006.04.006
16. Hasse U, Wagner K, Scholz F (2004) J Solid State Electrochem 8:842
17. Hasse U, Scholz F (2005) Electrochem Commun 7:173